Red States versus Blue States in Colloidal Silicon Nanocrystals: Exciton Sequestration into Low-Density Traps

ARTICLE *in* JOURNAL OF PHYSICAL CHEMISTRY LETTERS · OCTOBER 2013

Impact Factor: 7.46 · DOI: 10.1021/jz401896k

8 AUTHORS, INCLUDING:

Jack Fuzell
University of California, Davis
2 PUBLICATIONS **21** CITATIONS
SEE PROFILE

Erik Busby
Columbia University
14 PUBLICATIONS **152** CITATIONS
SEE PROFILE

Susan M Kauzlarich
University of California, Davis
399 PUBLICATIONS **6,642** CITATIONS
SEE PROFILE

Delmar S Larsen
University of California, Davis
86 PUBLICATIONS **2,706** CITATIONS
SEE PROFILE

THE JOURNAL OF PHYSICAL CHEMISTRY Letters

Letter

pubs.acs.org/JPCL

Red States versus Blue States in Colloidal Silicon Nanocrystals: Exciton Sequestration into Low-Density Traps

Jack Fuzell,[†] Arthur Thibert,[†] Tonya M. Atkins,[†] Mita Dasog,[‡] Erik Busby,[†] Jonathan G. C. Veinot,[‡,§] Susan M. Kauzlarich,[†] and Delmar S. Larsen*[,†]

[†]Department of Chemistry, University of California, Davis, One Shields Avenue, Davis, California 95616, United States

[‡]Department of Chemistry, University of Alberta, 11227 Saskatchewan Drive, Edmonton, Alberta T6G 2G2, Canada

[§]NRC National Institute for Nanotechnology, Edmonton, Alberta T6G 2M9, Canada

Supporting Information

ABSTRACT: The ultrafast exciton photodynamics of red-emitting and blue-emitting colloidal Si nanocrystals are contrasted under low (1.5 mJ/cm^2) and high (9.1 mJ/cm^2) excitation powers with broadband transient absorption spectroscopy. While the low-power initiated transient signals differ strongly for the two samples, the high-power signals exhibit similar nonmonotonic kinetics, resulting in a new population formed on a 10 to 30-ps time scale with a sample independent spectrum and decay kinetics. This phenomenon is ascribed to the saturation of low-density red-emitting and blue-emitting traps via a state-filling mechanism to populate new meta-stable states at higher excitation powers. The states responsible for blue emission and high-power populations are ascribed to traps from low-density nitrogen and oxygen impurities, respectively, and share similar charge-transfer character with the silicon nanocrystal core.

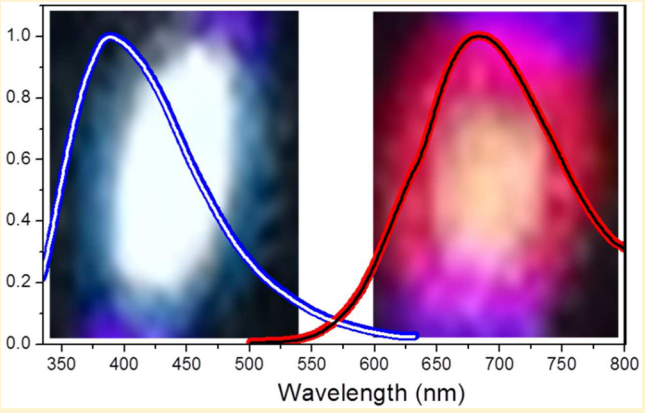

SECTION: Kinetics and Dynamics

The use of silicon in novel applications has been a topic of great research interest in the past few decades. Unlike many of the other semiconductor materials that often contain toxic elements like cadmium or lead, silicon is nontoxic and Earth abundant. Moreover, due to the long history of silicon use in the semiconductor industry, the infrastructure needed for its isolation, purification, and processing is well-developed. Silicon nanocrystals (NCs) are also a popularly studied material with potential applications in multiple fields including bioimaging,[1−5] nanophotonics,[6,7] and solar cells.[6,8] Although bulk silicon is an indirect band gap semiconductor and consequently a poor emitter of light, when it is prepared in a low dimensional state such as in NCs, it becomes an efficient light emitter. As the size of Si NC decreases, the electrons become quantum confined and the energy of the bandgap widens, the momentum states of the electrons spread out, and direct exciton recombination becomes allowed.[9,10]

Since the Bohr radius of photoinduced excitons in the NC can extend beyond the physical dimensions of the NC core, the surface conditions (including ligand character and traps) can significantly alter optical properties like photoluminescence. While the influence of NC surfaces in directing exciton dynamics in direct II−VI semiconductor NCs samples like CdSe and CdS has been extensively studied,[11−13] its role in influencing exciton dynamics in silicon NCs is still poorly understood. Because of the Si NCs strong potential for advancing newly developing materials, resolving the mechanisms that affect excitonic properties like photoluminescence (PL) for use as in vivo imaging probes and charge-separation and recombination for use in photovoltaic devices are of importance. For example, the origin of silicon NC photoluminescence remains the subject of much debate: is it from the recombination of trapped carriers on the surface states,[14,15] quantum confined excitons in the core of the particle,[10,16] or both?[17,18]

As with most semicoonduct NC samples, multiple approaches have emerged to prepare silicon NCs and can be broadly categorized into three classes: gas-phase,[19−21] solution-phase,[22−24] and solid state.[25] The synthesis methods can strongly influence surface and core atomic arrangements including absorption and emission spectra, depending on the starting material and the temperatures involved in the protocol.[26−28] The precursor chemicals used in many synthetic procedures may introduce low-density of impurities such as

Received: September 4, 2013
Accepted: October 21, 2013

   dx.doi.org/10.1021/jz401896k | J. Phys. Chem. Lett. 2013, 4, 3806−3812

Scheme 1. Synthesis Approaches for the Alkyl-Passivated Si NC Samples Used in This Study[a]

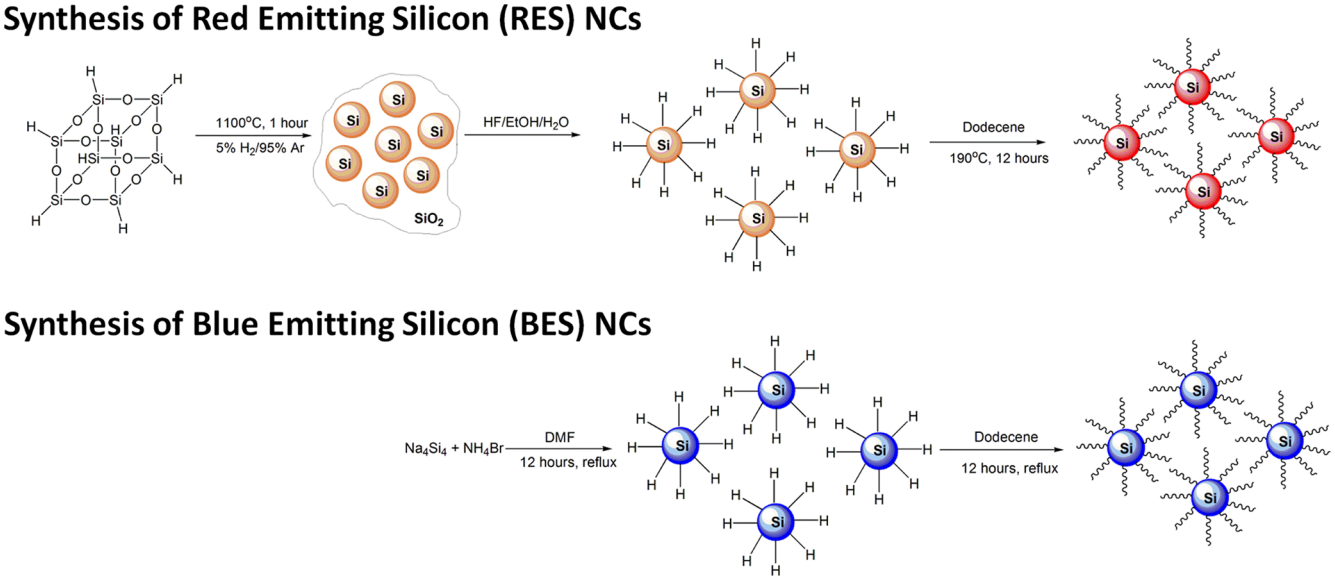

[a](Top) Synthesis of the red-emitting silicon (RES) NCs using silsesquioxane (HSQ). (Bottom) Synthesis of blue-emitting silicon (BES) NCs from the reduction of sodium silicide. Both samples were passivated with dodecene ligands and dissolved in toluene. Scheme adapted from ref 18.

nitrogen, and similarly, exposure of silicon NCs to O_2 has been proposed to form a SiO_x layer on the surface, which can induce a PL red-shift and reduce the PL efficiency due to faster defect-induced nonradiative recombination of excitons.[9,10,15,29−31] The PL of certain silicon NCs can be tuned throughout the red region of the visible spectrum by adjusting their size with smaller dots emitting at higher energies; since these Si NCs primarily emit in the red spectral region, they are termed RES for "red-emitting-silicon".[32] In contrast, silicon NCs synthesized from other protocols do not (or weakly) exhibit a size dependence of the PL and emit exclusively in the blue spectral range; these NCs are termed BES for "blue-emitting-silicon."[28,33]

While the mechanisms responsible for the different PL properties are still unclear, a recent study hypothesized that blue PL in BES NCs originates from nitrogen impurities introduced during their synthesis.[34] Ultrafast transient absorption (TA) spectroscopy is a powerful technique to directly characterize evolving exciton populations from photogeneration to recombination. TA signals have been used to characterize exciton dynamics in several colloidal silicon NCs samples, however, comparing the results from these studies can be difficult since the measured signals originate from the samples that are typically generated with differing synthetic protocols, or dissolved in different solvents, or capped with different ligand or are initiated under different conditions (e.g., excitation wavelengths, intensities or pulse widths). Here, we contrast the broadband TA signals of two colloidal silicon NC samples (BES and RES) synthesized with different protocols (Scheme 1), but otherwise are near identical samples. The silicon NCs in both samples are dodecene-capped and are dissolved in toluene under similar concentrations, and the TA signals were collected in back-to-back experiments under identical 400-nm excitation conditions (with two different excitation powers). The only difference other than synthetic protocols between the samples was that BES NCs were slightly larger (6 nm ±2 nm) than the RES NCs (3.5 ± 0.4 nm), but the differing sizes of the two samples is not a significant difference in the comparison since the emission of the BES NC samples do not vary greatly based on NC size (unpublished data).

The RES NCs were fabricated using the thermally induced disproportionation of hydrogen silsesquioxane (HSQ), while the BES NCs were synthesized using a solution reaction of sodium silicide with ammonium bromide. Transmission electron microscopy (TEM) shows that both silicon samples adopt a crystalline diamond structure. Complete characterization of the silicon NC samples used in this study has been published including EXAFS, XPS, XRD, HRTEM, SAED, EDX, STM, IR, Raman, UV−vis, PL.[28] We extend this comparison by directly characterizing the exciton photodynamics responsible for the differing PL emission with broadband TA spectroscopy coupled with global analysis.

Ultrafast exciton dynamics of porous silicon NCs typically exhibit biexponential decay kinetics with a fast (<1 ps) decay often attributed to exciton trapping and/or thermalization and the slower decay (30 to 100 ps) attributed to primary recombination pathways.[14,35,36] Similar exciton dynamics are resolved in colloidal NCs with organic capping ligands such as aminopropenyl,[37] ethenylthiophene,[32] vinylpyridine,[38] and vinylthiophene.[39] Each ligand confers different optical properties upon their silicon NC cores with some ligands acting as 'optical antennas' to absorb excitation light and generate silicon-ligand charge-transfer (CT) states, and other ligands can transfer electrons into the conduction band of the silicon NC either via photoinduced electron transfer or excitation energy transfer mechanisms.[32,38−40] For example, the aminopropenyl ligand greatly increased the photoinduced absorption of silicon NCs compared to NCs encapsulated in silica due to core-to-ligand charge transfer transitions.[37]

The UV−vis absorption and PL spectra of both BES and RES NCs are contrasted in Figure 1. The absorption spectra of both samples (solid curves) are qualitatively similar and extend from the UV to 500 nm with an exponential increase at higher photon energies; the RES NCs (solid red curve) exhibits a slightly faster rise.[37] In stark contrast, the PL of the two samples

dx.doi.org/10.1021/jz401896k | J. Phys. Chem. Lett. 2013, 4, 3806−3812

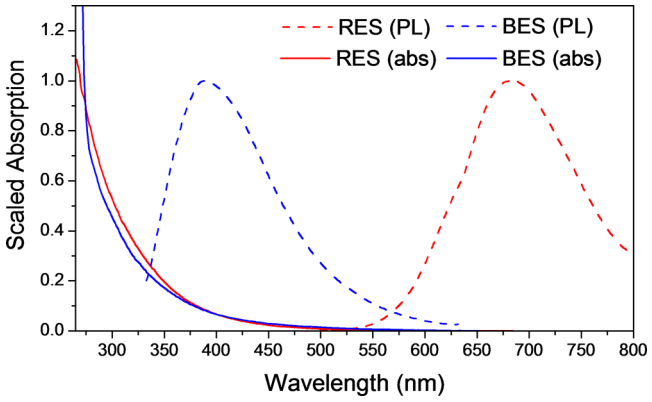

Figure 1. Normalized ground-state absorption (solid curves) and PL spectra (dashed curves) for RES (red curves) and BES (blue curves) NCs. All spectra were scaled to facilitate comparison. PL spectra were collected under 300-nm excitation. The energy resolved spectra are compared in Figure S1 (Supporting Information).

differ markedly with the BES NCs emitting at 390 nm with a 115-nm full width at half-maximum (fwhm; dashed blue curve) and the RES NCs emitting at 680 nm with a 140-nm fwhm (dashed red curve). The RES NCs also exhibit a weak shoulder in the PL spectrum at approximately 625 nm. When plotted on an energy scale (Figure S1, Supporting Information), the bandwidth of the BES PL (7500 cm^{-1}) is significantly broader than the RES PL spectrum (3000 cm^{-1}).

The TA spectra of both BES and RES samples exhibit broad positive induced absorptions (IA) extending across the entire visible range of probe wavelengths with no clearly resolved stimulated emission or bleach bands (Figure 2); however, they differ significantly with respect to the structure of the IA. The initial low-power spectrum (Figure 2A, black curve) of the RES NCs peaks in the blue (<435 nm) and red (>700 nm) regions with a depression around 550 nm. These early time (<5 ps) spectra are similar to previously measured exciton charge-transfer spectra between organic ligands and silicon NC cores,[32,38] although this photoreaction is unlikely with the RES and BES NCs studied here since they are both capped with inert dodecene ligands.[32,38,39] Interestingly, the spectral features of the BES low-power spectra are *inverted* from the RES spectra (Figures 2B and Figure S7) with a 550-nm peak and decreased IA on the spectral edges of the probe range. These low-power signals alone emphasize that the exciton dynamics for the two samples differ appreciably, but shed little light on the nature of the excitons, nor the mechanisms dictating their dynamics and resulting PL properties.

In contrast to the low-power TA spectra, the high-power signals for both BES and RES samples are appreciably more complex. The initial (<10 ps) high-power TA spectra (Figure 2C and 2D; black curves) strongly resemble their respective low-power counterparts (Figure 2A and 2B; black curves) for each sample, indicating that the differing nature of the nascent excitons for each sample is independent of incident excitation power. However, instead of decaying monotonically as in the low-intensity signals (Figure 3; filled curves), the initial high-power spectra of both samples evolve into new 'terminal' spectra that *differ* from the corresponding low-power spectra (Figure 2C,D, green curves) via *nonmonotonic* kinetics as demonstrated in the single wavelength traces (Figure 3; unfilled circles). These terminal populations exhibit spectra that peak at ~550 nm and resemble (but are not identical to) the low-power BES spectrum (Figure 2B). Despite the stark differences in the low-power spectra and kinetics, both silicon NC samples exhibit near identical high-power terminal spectra with identical (~20 ns) decay kinetics (Figure S7). This indicates that while the initial high-power populations differ for the two samples, the terminal populations induced by higher excitation powers are sample-independent and share a similar origin.

Multiwavelength global analysis was used to fit the broadband TA signals to a three-population sequential model

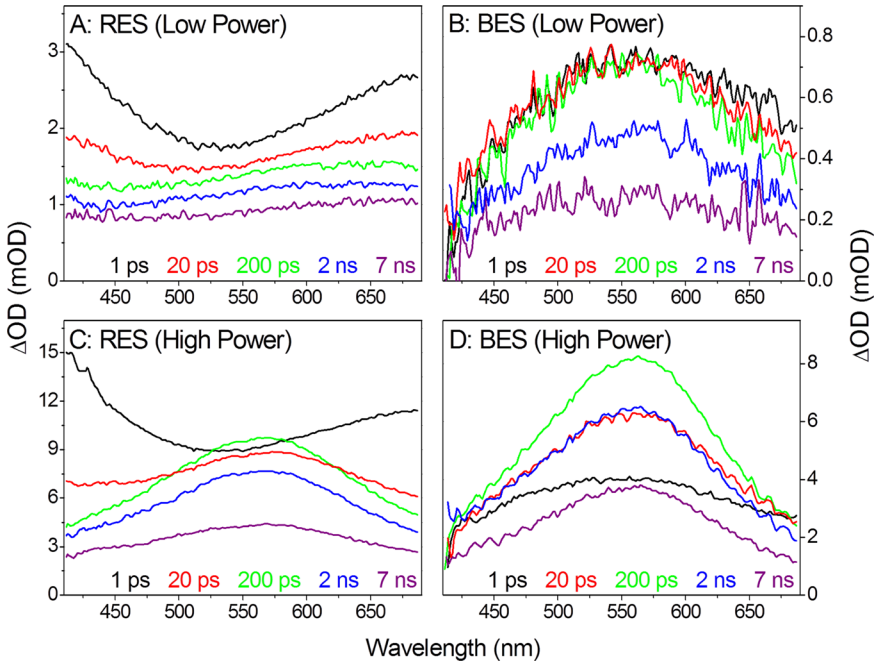

Figure 2. Transient spectra at select times after 400-nm excitation of both RES (left curves) and BES (right curves) in toluene under low-excitation density of 1.5 mJ/cm^2 (top) and high-excitation density 9.1 mJ/cm^2 (bottom).

dx.doi.org/10.1021/jz401896k | J. Phys. Chem. Lett. 2013, 4, 3806−3812

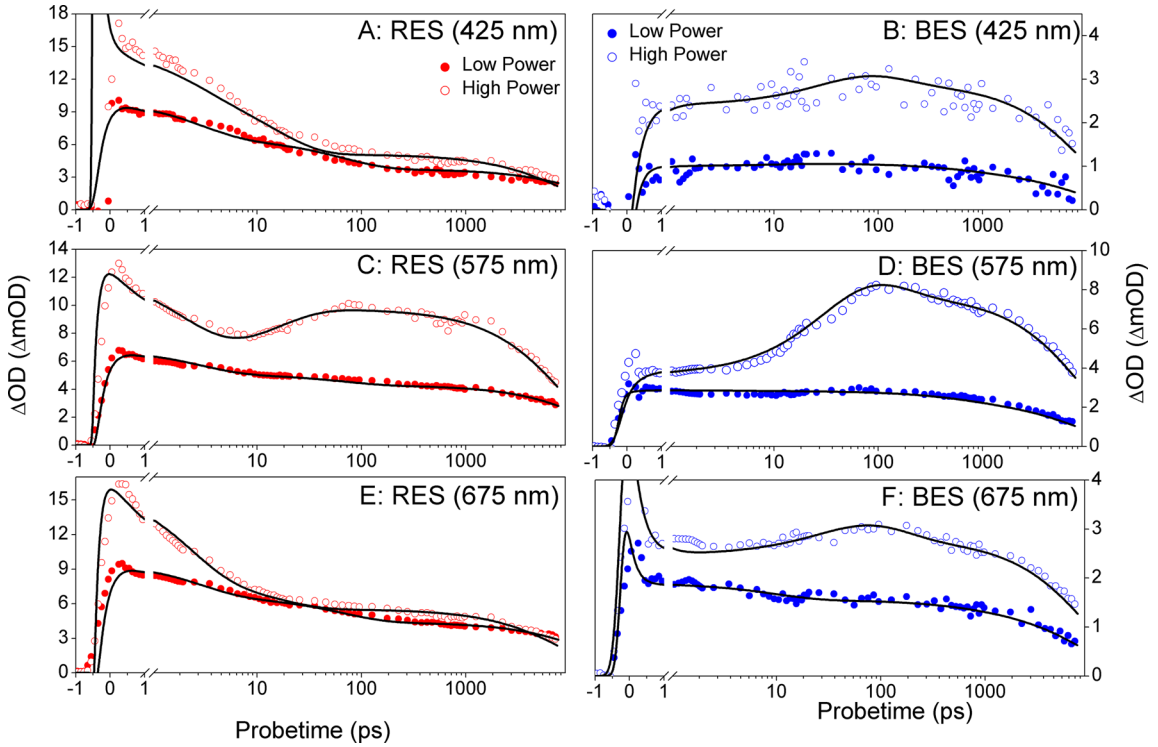

Figure 3. Transient kinetics for RES (A, C, E) (red curves) and BES (B, D, F) (blue curves) NCs. The low excitation power signals (filled circles) are scaled to compare to the high power (unfilled circles) 3-fold for the RES NCs and 4-fold for the BES NCs samples. The TA data in panels A, E, and F contain coherent artifacts (cross-phase modulation) that extend beyond the scale and are not shown to facilitate comparison of data. Note, the time axis scales linearly to 1 ps and then logarithmical afterward. Solid lines are fits from the sequential global analysis outlined in Figures S3−S6.

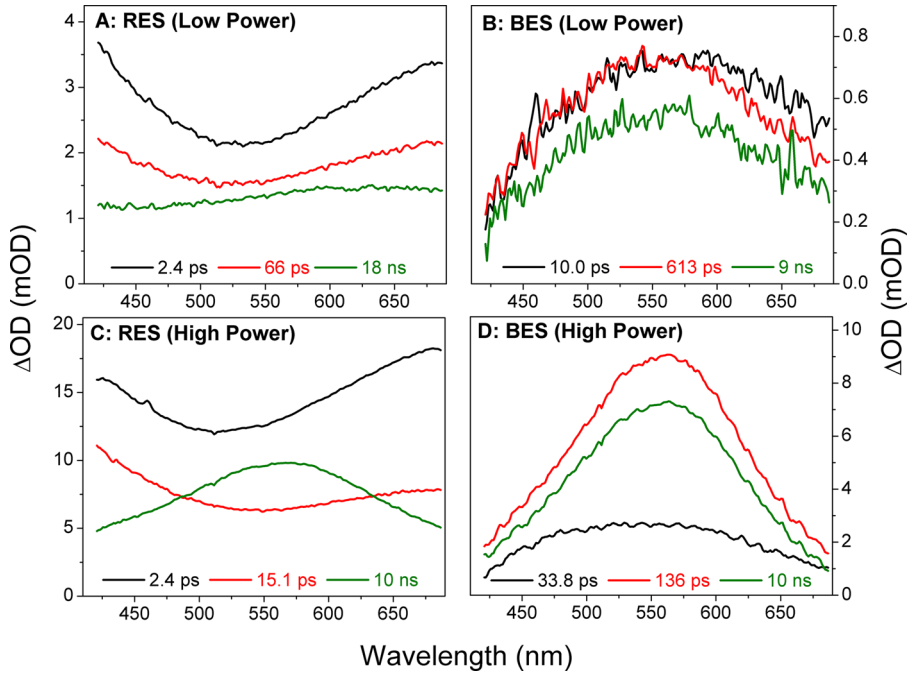

Figure 4. Estimated EADS extracted from global analysis of the transient data outlined in Figures S3−S6. The EADS are labeled by their corresponding time constants (EADS1 (black curves), EADS2 (red curves) and EADS3 (green curves). The spectrum describing the instrument-limited coherent artifacts are not shown.

(EADS1 → EADS2 → EADS3 →) with constituent populations exhibiting fixed spectra (called Evolutionary Associated Difference Spectra or EADS) with exponentially evolving amplitudes. This analysis (Figure 4) fits the experimental data well (Figure 3, black curves) with errors estimated at approximately 5% for time constants and 5% for amplitudes (i.e., spectrum). The low-power signals (filled circles) for both samples exhibit monotonic decay kinetics with a terminal population (EADS3) that persists beyond the 8-ns time window of the experiment (~18 and 10 ns for RES and

dx.doi.org/10.1021/jz401896k | J. Phys. Chem. Lett. 2013, 4, 3806−3812

BES, respectively). The RES NCs exhibit a faster initial decay than the BES NCs, which is due to both increased Auger recombination kinetics between the samples since the exciton density is higher in these signals (based on the signal amplitude) and to intrinsic sample-dependent kinetics. The high-power signals (unfilled circles) for both samples exhibit nonmonotonic kinetics with "terminal populations" (EADS3) that are generated on a 15-ps (RES) and 34-ps (BES) time scale and then decay near exponentially on a >10-ns time scale. The strong spectral and kinetic similarities of the terminal populations (EADS3) in both silicon NC samples argues for a shared sample-independent origin of this population.

Nonlinear power-dependent kinetics are ubiquitous in NC studies, including both porous silicon and colloidal silicon NC samples and have been ascribed to different phenomena. Klimov et al.[14] resolved power-dependent kinetics (0.1−5.5 mJ/cm^2) of silicon NCs obtained from the annealing of ion implanted oxides. They observed a nonlinear power dependence of the decay kinetics that was ascribed to the re-excitation of the initial exciton population. Their signals were fit to a biexponential model (with time constants 1.5 and 8 ps) and it was observed that the amplitude of the faster component was relatively greater at elevated excitation intensities than the slower component. A similar trend was also observed by Groenewegen et al.[39] with colloidal silicon NCs terminated with 3-vinylthiophene, who also resolved biexponential kinetics (0.6 and 1.6 ps) with excitation densities ranging from 72 to 285 μJ/cm^2. They resolved monotonically decaying signals with greater amplitude of the 0.6-ps kinetics versus the 1.6-ps phase as the excitation power was increased. Such decay dynamics often originate from Auger recombination pathways including both two-particle[41] or three-particle[42] mechanisms, when more than one excitation is generated per NC (i.e., higher excitation powers). This nonlinear mechanism results *faster* decay kinetics (but still monotonic) under increased excitation powers and is rarely responsible for the growth of a new population like that observed in the BES and RES data in Figures 2−4.

Klimov and co-workers invoked an Auger recombination mechanism to account for the high-excitation power generation of a new population via the promotion of holes into deeper surface traps in noncolloidal CdS NCs.[41,43] While this mechanism does exhibit a nonlinear excitation power dependence expected for the generation of deeper trap species, it is most active when the exciton density is greatest (i.e., initially after excitation). Hence, this mechanism is not responsible for the delayed (15-ps to 30-ps) growth of the terminal population in the silicon NC data presented here (Figure 4C,D).

An alternative mechanism is that higher excitation intensities may directly excite the dodecene ligand via a two- or multiphoton absorption, which may then initiate an energy or charge transfer reaction with the silicon NC core. This was observed by Kryschi and co-workers for several organic ligand terminated silicon NCs.[32,38,39] While, this mechanism is capable of generating delayed dynamics, which are dictated by the intrinsic energy or electron transfer kinetics of the delayed reaction, the similarity between the initial spectra (EADS1) for both low and high-power signals (Figure 4; black curves) indicates that no new photogenerated population (i.e., an excited dodecene* population) is directly photogenerated by high-power excitation pulses as required by this mechanism.

The preferred mechanism (Figure 5) to describe the power dependence of the TA signals for both RES and BES NCs is that under low-power excitation, excitons are rapidly localized

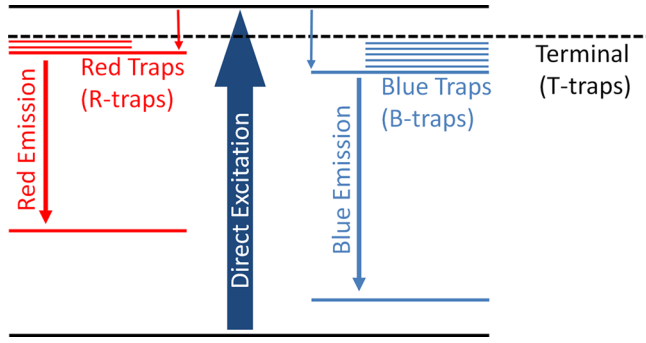

Figure 5. Simplified scheme of photodynamics of RES (red) and BES (blue) NCs. Three distinct species are resolved. The low density of both red and blue traps result in the sensitivity to incident photo flux results (site-filling) whereby samples with multiple excitons persist to exhibit charge-separated dynamics (identical for both RES and BES samples).

in traps (R-traps and B-traps for RES and BES NCs, respectively), that are bright and emit in the corresponding spectral regions characteristic of the NCs. Both traps are observed with a low density, so that elevated excitation densities can "fill" or saturate the available traps and generate the new terminal population(s), which we also posit as a trapped state (T-trap). Hence, the state-filling behavior of each sample results in nonmonotonic kinetics as excitons fill the low-density traps and eventually locate and localize at T-traps. Similar state-filling models have been used to interpret time-resolved PL experiments with the appearance of higher-energy populations in silicon NCs embedded within a SiO_2 matrix and indium/gallium/arsenide NCs grown on a gallium arsenide substrates.[44,45]

While the connectivity of the R-traps, B-traps, and T-traps is suggested from the power-dependent TA signals, identifying their nature requires comparison of the chemical composition of the NCs. X-ray photoelectron spectroscopy (XPS) identified the presence of nitrogen only for the BES NCs,[28] and it was shown that RES NCs can be converted to BES NCs when nitrogen containing ligands are added to the solution. For this reason, the B-traps are ascribed to nitrogen defects and are responsible for the blue emission in BES NCs. Since computational studies indicate that nitrogen atoms can diffuse rapidly through the bulk silicon until they become trapped at the surface, it is likely that the B-traps are surface nitrogen defects.[46,47] This is further supported by solvatochromism studies that show that these nitrogen traps result in a charge-transfer with the silicon NC core and are exposed to the solvent.[28,33]

The Fourier transform infrared (FTIR) spectra of both samples have resolved Si−O stretches,[28] which indicates a second impurity, but is a shared feature of both BES and RES samples. The strong similarity of exciton spectra (Figures 4 and S7) and dynamics (Figure S3) for the nitrogen B-traps and the terminal T-traps spectra suggest that both traps exhibit similar charge-transfer character. Oxygen defects have been known to induce red-shifting PL and reduce the PL efficiency due faster defect-induced nonradiative recombination of excitons.[9,10,15,29−31] Hence, the terminal populations are ascribed to oxygen impurities that generate deeper traps and are populated upon saturation of the R- and B-traps in both RES and BES NC samples, respectively, upon higher excitation powers.

dx.doi.org/10.1021/jz401896k | J. Phys. Chem. Lett. 2013, 4, 3806−3812

The oxygen-based T-traps (Figure 4C,D; green curves), and the nitrogen-based B-traps (Figure 4B) differ strongly from the characteristic spectrum of the R-traps (Figure 4A; black curves), which suggests that the R-traps may be more covalent in nature or are most strongly perturbed by the surface. The TA spectra are consistent with the idea of increased surface trapping for the R-traps are due to ligand effects in the RES NCs since large surface trapping effects often appear in TA signals as a broadband IA to the red of the band edge exciton in NC (Figure 4A; black curve). This is further support by the faster Auger recombination time scales in the RES NCs that are distinctly faster than the BES NCs (Figure 4), which is consistent with greater surface effects and trapping.[48] Other signatures of trapping of excitons include impulsively launching coherent phonons (if trapped fast enough),[49] which were not resolved in the TA data presented here.

The large bandwidth of the PL (Figures 1 and S1), especially of the BES NCs, supports this trapping hypothesis, as such PL is commonly associated with some large distribution of mid gap defects. The PL from traps is better understood in terms of charge transfer from the core to the surface of the NC, which yields a large polarization and produces a stronger phonon coupling and therefore broad PL. Hence, the surface chemistry, including surface traps, dictates the charge transfer dynamics and thus the resulting PL. While this has been explore in detail in II–VI semiconductor NCs, the applicability of such a picture for the silicon NCs studied here is not yet established, although it's likely similar.[50]

To conclude, ultrafast transient absorption dynamics were measured and compared for two colloidal dodecene-capped silicon nanocrystals produced under differing synthetic protocols, but under otherwise identical experimental conditions. These two silicon samples exhibit either red or blue PL upon excitation, and the subsequent resolved exciton dynamics and spectra for both samples differ greatly under low excitation powers, but upon elevated excitation powers exhibit the delayed generation of a new terminal exciton population. This phenomenon is ascribed to the site-filling of low-density traps from nitrogen impurities (for blue-emission) and unknown R-trap to populate deeper traps involving oxygen impurities. The nature of the traps responsible for the red emission is unclear, but differs from the charge-transfer characteristics of the nitrogen and oxygen traps. A more extensive study involving characterizing the exciton dynamics of silicon NCs with a greater range of sizes and excitation powers, with differing surface compositions, varying ligands and different solvents is currently in preparation.

■ ASSOCIATED CONTENT

Supporting Information

Detailed synthesis protocols and additional transient data. This material is available free of charge via the Internet at http://pubs.acs.org.

■ AUTHOR INFORMATION

Corresponding Author

*E-mail: dlarsen@ucdavis.edu.

Notes

The authors declare no competing financial interest.

■ ACKNOWLEDGMENTS

This research was supported by an NSF (DMR-1035468) grant to S.M.K. and D.S.L. J.G.C.V. acknowledges funding from the Natural Sciences and Engineering Research Council of Canada (NSERC), Canada Foundation for Innovation (CFI), Alberta Science and Research Investment Program (ASRIP), Alberta Innovates Technology Futures (AITF), and University of Alberta Department of Chemistry.

■ REFERENCES

(1) Erogbogbo, F.; Tien, C.-A.; Chang, C.-W.; Yong, K.-T.; Law, W.-C.; Ding, H.; Roy, I.; Swihart, M. T.; Prasad, P. N. Bioconjugation of Luminescent Silicon Quantum Dots for Selective Uptake by Cancer Cells. *Bioconjugate Chem.* **2011**, *22*, 1081–1088.

(2) Erogbogbo, F.; Yong, K.-T.; Roy, I.; Xu, G.; Prasad, P. N.; Swihart, M. T. Biocompatible Luminescent Silicon Quantum Dots for Imaging of Cancer Cells. *ACS Nano* **2008**, *2*, 873–878.

(3) Pons, T.; Pic, E.; Lequeux, N.; Cassette, E.; Bezdetnaya, L.; Guillemin, F.; Marchal, F.; Dubertret, B. Cadmium-Free CuInS2/ZnS Quantum Dots for Sentinel Lymph Node Imaging with Reduced Toxicity. *ACS Nano* **2010**, *4*, 2531–2538.

(4) Kouki, F.; Masaki, H.; Keisuke, S.; Noriyoshi, M.; Ryosuke, M.; Sanshiro, H.; Akiyoshi, H.; Richard, D. T.; Yoshinobu, M.; Kenji, H.; Kenji, Y. Luminescent Passive-Oxidized Silicon Quantum Dots as Biological Staining Labels and Their Cytotoxicity Effects at High Concentration. *Nanotechnology* **2008**, *19*, 415102.

(5) Zhang, X.; Brynda, M.; Britt, R.; Carroll, E.; Larsen, D.; Louie, A.; Kauzlarich, S. Synthesis and Characterization of Manganese-Doped Silicon Nanoparticles: Bifunctional Paramagnetic-Optical Nanomaterial. *J. Am. Chem. Soc.* **2007**, *129*, 10668–10669.

(6) Huang, W.-Q.; Liu, S.-R.; Qin, C.-J.; Lü, Q.; Xu, L. Nano-Laser on Silicon Quantum Dots. *Opt. Commun.* **2011**, *284*, 1992–1996.

(7) Pavesi, L.; Dal Negro, L.; Mazzoleni, C.; Franzo, G.; Priolo, F. Optical Gain in Silicon Nanocrystals. *Nature* **2000**, *408*, 440–444.

(8) Beard, M. C.; Knutsen, K. P.; Yu, P.; Luther, J. M.; Song, Q.; Metzger, W. K.; Ellingson, R. J.; Nozik, A. J. Multiple Exciton Generation in Colloidal Silicon Nanocrystals. *Nano Lett.* **2007**, *7*, 2506–2512.

(9) Ledoux, G.; Guillois, O.; Porterat, D.; Reynaud, C.; Huisken, F.; Kohn, B.; Paillard, V. Photoluminescence Properties of Silicon Nanocrystals as a Function of Their Size. *Phys. Rev. B* **2000**, *62*, 15942–15951.

(10) Garoufalis, C. S.; Zdetsis, A. D.; Grimme, S. High Level Ab Initio Calculations of the Optical Gap of Small Silicon Quantum Dots. *Phys. Rev. Lett.* **2001**, *87*, 276402.

(11) Jones, M.; Scholes, G. D. On the Use of Time-Resolved Photoluminescence as a Probe of Nanocrystal Photoexcitation Dynamics. *J. Mater. Chem.* **2010**, *20*, 3533–3538.

(12) Chuang, C.-H.; Doane, T. L.; Lo, S. S.; Scholes, G. D.; Burda, C. Measuring Electron and Hole Transfer in Core/Shell Nanoheterostructures. *ACS Nano* **2011**, *5*, 6016–6024.

(13) Kambhampati, P. Hot Exciton Relaxation Dynamics in Semiconductor Quantum Dots: Radiationless Transitions on the Nanoscale. *J. Phys. Chem. C* **2011**, *115*, 22089–22109.

(14) Klimov, V. I.; Schwarz, C. J.; McBranch, D. W.; White, C. W. Initial Carrier Relaxation Dynamics In Ion-Implanted Si Nanocrystals: Femtosecond Transient Absorption Study. *Appl. Phys. Lett.* **1998**, *73*, 2603–2605.

(15) Wolkin, M. V.; Jorne, J.; Fauchet, P. M.; Allan, G.; Delerue, C. Electronic States and Luminescence in Porous Silicon Quantum Dots: The Role of Oxygen. *Phys. Rev. Lett.* **1999**, *82*, 197–200.

(16) Kovalev, D.; Heckler, H.; Polisski, G.; Koch, F. Optical Properties of Si Nanocrystals. *Phys. Status Solidi B* **1999**, *215*, 871–932.

(17) Trojanek, F.; Neudert, K.; Maly, P.; Dohnalova, K.; Pelant, I. Ultrafast Photoluminescence In Silicon Nanocrystals Studied by Femtosecond Up-Conversion Technique. *J. Appl. Phys.* **2006**, *99*, 116108–3.

(18) Sykora, M.; Mangolini, L.; Schaller, R. D.; Kortshagen, U.; Jurbergs, D.; Klimov, V. I. Size-Dependent Intrinsic Radiative Decay Rates of Silicon Nanocrystals at Large Confinement Energies. *Phys. Rev. Lett.* **2008**, *100*, 067401.
(19) Pi, X. D.; Liptak, R. W.; Deneen Nowak, J.; Wells, N. P.; Carter, C. B.; Campbell, S. A.; Kortshagen, U. Air-Stable Full-Visible-Spectrum Emission from Silicon Nanocrystals Synthesized by an All-Gas-Phase Plasma Approach. *Nanotechnology* **2008**, *19*, 245603–245618.
(20) Mangolini, L.; Jurbergs, D.; Rogojina, E.; Kortshagen, U. Plasma Synthesis and Liquid-Phase Surface Passivation of Brightly Luminescent Si Nanocrystals. *J. Lumin* **2006**, *121*, 327–334.
(21) Li, X.; He, Y.; Talukdar, S. S.; Swihart, M. T. Process for Preparing Macroscopic Quantities of Brightly Photoluminescent Silicon Nanoparticles with Emission Spanning the Visible Spectrum. *Langmuir* **2003**, *19*, 8490–8496.
(22) Neiner, D.; Chiu, H. W.; Kauzlarich, S. M. Low-Temperature Solution Route to Macroscopic Amounts of Hydrogen Terminated Silicon Nanoparticles. *J. Am. Chem. Soc.* **2006**, *128*, 11016–11017.
(23) Pettigrew, K. A.; Liu, Q.; Power, P. P.; Kauzlarich, S. M. Solution Synthesis of Alkyl- and Alkyl/Alkoxy-Capped Silicon Nanoparticles via Oxidation of Mg_2Si. *Chem. Mater.* **2003**, *15*, 4005–4011.
(24) Yang, C.-S.; Bley, R. A.; Kauzlarich, S. M.; Lee, H. W. H.; Delgado, G. R. Synthesis of Alkyl-Terminated Silicon Nanoclusters by a Solution Route. *J. Am. Chem. Soc.* **1999**, *121*, 5191–5195.
(25) Hessel, C. M.; Henderson, E. J.; Veinot, J. G. C. Hydrogen Silsesquioxane: A Molecular Precursor for Nanocrystalline $Si–SiO_2$ Composites and Freestanding Hydride-Surface-Terminated Silicon Nanoparticles. *Chem. Mater.* **2006**, *18*, 6139–6146.
(26) Draeger, E. W.; Grossman, J. C.; Williamson, A. J.; Galli, G. Influence of Synthesis Conditions on the Structural and Optical Properties of Passivated Silicon Nanoclusters. *Phys. Rev. Lett.* **2003**, *90*, 167402.
(27) Draeger, E. W.; Grossman, J. C.; Williamson, A. J.; Galli, G. Synthesis Dynamics of Passivated Silicon Nanoclusters. *Phys. Status Solidi B* **2003**, *239*, 11–18.
(28) Dasog, M.; Yang, Z.; Regli, S.; Atkins, T. M.; Faramus, A.; Singh, M. P.; Muthuswamy, E.; Kauzlarich, S. M.; Tilley, R. D.; Veinot, J. G. C. Chemical Insight into the Origin of Red and Blue Photoluminescence Arising from Freestanding Silicon Nanocrystals. *ACS Nano* **2013**, *7* (3), 2676–2685.
(29) Dohnalová, K.; Fučíková, A.; Umesh, C. P.; Humpolíčková, J.; Paulusse, J. M. J.; Valenta, J.; Zuilhof, H.; Hof, M.; Gregorkiewicz, T. Microscopic Origin of the Fast Blue-Green Luminescence of Chemically Synthesized Non-oxidized Silicon Quantum Dots. *Small* **2012**, *8*, 3185–91.
(30) Garoufalis, C. S.; Zdetsis, A. D. High Accuracy Calculations of the Optical Gap and Absorption Spectrum of Oxygen Contaminated Si Nanocrystals. *Phys. Chem. Chem. Phys.* **2006**, *8*, 808–813.
(31) Kanemitsu, Y.; Okamoto, S.; Otobe, M.; Oda, S. Photoluminescence Mechanism in Surface-Oxidized Silicon Nanocrystals. *Phys. Rev. B* **1997**, *55*, R7375–R7378.
(32) Cimpean, C.; Groenewegen, V.; Kuntermann, V.; Sommer, A.; Kryschi, C. Ultrafast Exciton Relaxation Dynamics in Silicon Quantum Dots. *Laser Photonics Rev.* **2009**, *3*, 138–145.
(33) Dal Negro, L.; Hamel, S.; Zaitseva, N.; Jae Hyung, Y.; Williamson, A.; Stolfi, M.; Michel, J.; Galli, G.; Kimerling, L. C. Synthesis, Characterization, and Modeling of Nitrogen-Passivated Colloidal and Thin Film Silicon Nanocrystals. *IEEE J. Sel. Top. Quant. Electron.* **2006**, *12*, 1151–1163.
(34) Hiller, D.; Goetze, S.; Munnik, F.; Jivanescu, M.; Gerlach, J. W.; Vogt, J.; Pippel, E.; Zakharov, N.; Stesmans, A.; Zacharias, M. Nitrogen at the Si-Nanocrystal/SiO_2 Interface and Its Influence on Luminescence and Interface Defects. *Phys. Rev. B* **2010**, *82*, 195401.
(35) Klimov, V.; McBranch, D.; Karavanskii, V. Strong Optical Nonlinearities in Porous Silicon: Femtosecond Nonlinear Transmission Study. *Phys. Rev. B* **1995**, *52*, R16989–R16992.
(36) Owrutsky, J. C.; Rice, J. K.; Guha, S.; Steiner, P.; Lang, W. Ultrafast Absorption in Free-Standing Porous Silicon Films. *Appl. Phys. Lett.* **1995**, *67*, 1966–1968.
(37) Atkins, T. M.; Thibert, A.; Larsen, D. S.; Dey, S.; Browning, N. D.; Kauzlarich, S. M. Femtosecond Ligand/Core Dynamics of Microwave-Assisted Synthesized Silicon Quantum Dots in Aqueous Solution. *J. Am. Chem. Soc.* **2011**, *133*, 20664–20667.
(38) Sommer, A.; Cimpean, C.; Kunz, M.; Oelsner, C.; Kupka, H. J.; Kryschi, C. Ultrafast Excitation Energy Transfer in Vinylpyridine Terminated Silicon Quantum Dots. *J. Phys. Chem. C* **2011**, *115*, 22781–22788.
(39) Groenewegen, V.; Kuntermann, V.; Haarer, D.; Kunz, M.; Kryschi, C. Excited-State Relaxation Dynamics of 3-Vinylthiophene-Terminated Silicon Quantum Dots. *J. Phys. Chem. C* **2010**, *114*, 11693–11698.
(40) Kuntermann, V.; Cimpean, C.; Brehm, G.; Sauer, G.; Kryschi, C.; Wiggers, H. Femtosecond Transient Absorption Spectroscopy of Silanized Silicon Quantum Dots. *Phys. Rev. B* **2008**, *77*, 115343.
(41) Htoon, H.; Hollingsworth, J. A.; Dickerson, R.; Klimov, V. I. Effect of Zero- to One-Dimensional Transformation on Multiparticle Auger Recombination in Semiconductor Quantum Rods. *Phys. Rev. Lett.* **2003**, *91*, 227401.
(42) Klimov, V. I.; Mikhailovsky, A. A.; McBranch, D. W.; Leatherdale, C. A.; Bawendi, M. G. Quantization of Multiparticle Auger Rates in Semiconductor Quantum Dots. *Science* **2000**, *287*, 1011–1013.
(43) Klimov, V. I.; McBranch, D. W. Auger-Process-Induced Charge Separation in Semiconductor Nanocrystals. *Phys. Rev. B* **1997**, *55*, 13173–13179.
(44) Raymond, S.; Fafard, S.; Poole, P. J.; Wojs, A.; Hawrylak, P.; Charbonneau, S.; Leonard, D.; Leon, R.; Petroff, P. M.; Merz, J. L. State Filling and Time-Resolved Photoluminescence of Excited States in $In_xGa_{1-x}As$/GaAs Self-Assembled Quantum Dots. *Phys. Rev. B* **1996**, *54*, 11548–11554.
(45) Wen, X. M.; Dao, L. V.; Hannaford, P.; Mokkapati, S.; Tan, H. H.; Jagadish, C. The State Filling Effect in P-Doped in InGaAs/GaAs Quantum Dots. *J. Phys.: Condens. Matter* **2007**, *19*, 386213.
(46) Schultz, P. A.; Nelson, J. S. Fast Through-Bond Diffusion of Nitrogen in Silicon. *App. Phys. Lett.* **2001**, *78*, 736.
(47) Goss, J. P.; Hahn, I.; Jones, R.; Briddon, P.; Öberg, S. Vibrational Modes and Electronic Properties of Nitrogen Defects in Silicon. *Phys. Rev. B: Condens. Matter Mater. Phys.* **2003**, *67*, 45206.
(48) Tyagi, P.; Kambhampati, P. False Multiple Exciton Recombination and Multiple Exciton Generation Signals in Semiconductor Quantum Dots Arise from Surface Charge Trapping. *J. Chem. Phys.* **2011**, *134*, 094706–10.
(49) Saari, J. I.; Dias, E. A.; Reifsnyder, D.; Krause, M. M.; Walsh, B. R.; Murray, C. B.; Kambhampati, P. Ultrafast Electron Trapping at the Surface of Semiconductor Nanocrystals: Excitonic and Biexcitonic Processes. *J. Phys. Chem. B* **2012**, *117*, 4412–4421.
(50) Mooney, J.; Krause, M. M.; Saari, J. I.; Kambhampati, P. Challenge to the Deep-Trap Model of the Surface in Semiconductor Nanocrystals. *Phys. Rev. B* **2013**, *87*, 081201.